On the Influence of Interactions between Phases on the Mechanical Stability of Retained Austenite in Transformation-Induced Plasticity Multiphase Steels

P.J. JACQUES, J. LADRIÈRE, and F. DELANNAY

The mechanical stability of dispersed retained austenite, *i.e.*, the resistance of this austenite to mechanically induced martensitic transformation, was characterized at room temperature on two steels which differed by their silicon content. The steels had been heat treated in such a way that each specimen presented the same initial volume fraction of austenite and the same austenite grain size. Nevertheless, depending on the specimen, the retained austenite contained different amounts of carbon and was surrounded by different phases. Measurements of the variation of the volume fraction of untransformed austenite as a function of uniaxial plastic strain revealed that, besides the carbon content of retained austenite, the strength of the other phases surrounding austenite grains also influences the austenite resistance to martensitic transformation. The presence of thermal martensite together with the silicon solid-solution strengthening of the intercritical ferrite matrix can "shield" austenite from the externally applied load. As a consequence, the increase of the mechanical stability of retained austenite is not solely related to the decrease of the M_s temperature induced by carbon enrichment.

I. INTRODUCTION

THE transformation-induced plasticity (TRIP) effect, *i.e.*, the mechanically induced martensitic transformation of metastable austenite, has been proven for many years to contribute very effectively to the deformation process in a large variety of fully austenitic iron-based alloys. Numerous studies have shown that the TRIP effect improves strength and ductility by helping to maintain a high work-hardening rate during straining.[1–11] This phenomenon is commonly ascribed to two different mechanisms:[12,13] (1) the stress-assisted nucleation of martensitic variants favorably oriented with respect to the applied stress (Magee effect[14] or orientation effect); and (2) the plastic straining of the surrounding phases due to the volume and shape changes associated with the displacive transformation (Greenwood–Johnson effect[15] or accommodation effect). In Fe-Ni-Cr alloys,[2,16,17] Fe-Ni alloys,[17,18] or in other highly alloyed fully austenitic steels,[3,19] tensile strength and elongation are enhanced when the chemical composition is such that the M_s temperature is just below the testing temperature.

The TRIP effect is also thought to be the main phenomenon responsible for the improved balance of strength and ductility exhibited by the new and so-called "TRIP-assisted multiphase steels." These low-alloy C-Mn-Si steels are quite different from the previous fully austenitic TRIP steels. They present a multiphase microstructure consisting of an intercritical ferrite matrix with a dispersion of bainite, metastable retained austenite, and martensite. In the present case, retained austenite is a minor phase ($\sim$5 to 20 pct[20]) dispersed in a ferrite-based microstructure. Previous studies[21–24] have shown that the enhancement of both strength and ductility in these TRIP-aided steels is related to the presence of this retained austenite, which transforms into martensite during mechanical straining.

In the case of cold-rolled steel sheets, the particular microstructure of the TRIP-assisted multiphase steels is obtained by carrying out a two-stage heat treatment. As for dual-phase steels, the first stage consists of an intercritical annealing, during which part of the initial microstructure transforms into austenite. While dual-phase steels are directly quenched to room temperature, TRIP-aided steels are rapidly cooled to a temperature at which an isothermal bainitic holding is conducted (typically in the range from 350 °C to 450 °C). During this second isothermal dwell, part of the intercritical austenite transforms to bainite, whereas the remaining austenite is stabilized in such a way that it does not transform to martensite during the final water quench to room temperature. The stabilization of austenite during the partial bainite transformation is due to carbon rejection from bainitic ferrite into residual austenite and to the inhibition of cementite precipitation from austenite when the steel contains enough silicon. It is well known that the displacive growth of upper-bainitic ferrite is followed by rejection of the excess carbon from bainitic ferrite into surrounding residual austenite, where cementite precipitation occurs.[25] This cementite precipitation can be totally inhibited in the presence of silicon (typically around 2 wt pct), since silicon has a very low solubility in cementite. As a consequence, the bainite transformation leads to the formation of a mixture of carbide-free bainitic ferrite and carbon-rich residual austenite. The high content of carbon in this residual austenite brings the M_s temperature below room temperature.[26] As a consequence, despite the effect of silicon on the activity of carbon in both ferrite and austenite, conventional TRIP-assisted multiphase steels always contain 1.5 to 2.5 wt pct silicon in order to prevent cementite precipitation. They also contain from 0.1 to 0.4 wt pct carbon and from 1.5 to 2.5 wt pct manganese (to improve hardenability).

P.J. JACQUES, Associate Researcher, and F. DELANNAY, Professor, Division of Physical Chemistry and Engineering of Materials, and J. LADRIÈRE, Professor, Division of Inorganic and Nuclear Chemistry, are with the Catholic University of Louvain, B-1348 Louvain-la-Neuve, Belgium.

Manuscript submitted May 16, 2000.

The present literature dealing with TRIP-assisted multiphase steels has not completely elucidated how the TRIP effect influences the mechanical properties and, especially, which parameters control the mechanical stability of retained austenite when this austenite is dispersed in a ferrite-based microstructure. While some studies have shown that the improvement of mechanical properties is primarily related to the initial volume fraction of retained austenite (which increases with increasing contents of carbon, silicon, and manganese),[22,27–29] other studies have shown that not only the volume fraction but also the stability of retained austenite must be taken into account.[22,29,30] A superior strength-ductility balance is attained when the strain-induced transformation of austenite develops gradually during plastic straining. Austenite stability is commonly ascribed to different parameters such as the presence of stabilizing elements like carbon or the reduction of austenite grain size. Whereas Sugimoto *et al.*[31] and Itami *et al.*[32] have shown that the morphology of retained austenite influences its stability, hardly anything has been reported on the possible influence of the other phases surrounding retained austenite.

A recent study[33] has demonstrated that large amounts of austenite can be retained after a two-stage heat treatment of a 0.16 wt pct C, 1.30 wt pct Mn steel containing only 0.38 wt pct silicon (*i.e.*, a typical dual-phase steel composition). Up to 10 pct of the austenite was shown to be retained after a short bainitic holding. In contrast to conventional high-silicon TRIP-aided steels, retained austenite, bainite, and martensite (and not only retained austenite and bainite) are present together with the intercritical ferrite matrix in this steel grade. It was shown that this martensite favorably influences mechanical properties by contributing to the strengthening of the steel. It was, therefore, concluded that both a TRIP effect and a composite strengthening effect contribute to enhance mechanical properties. Although the mechanical properties exhibited by that low-silicon steel are quite remarkable when compared to the properties of dual-phase steels or of solid-solution and precipitation-hardened high-strength steels, they remain lower than the properties of conventional high-silicon TRIP-assisted multiphase steels with the same global carbon content. Indeed, in comparison with a conventional TRIP-aided steel grade differing only by a higher silicon content,[34] the true stress at maximum load and the true uniform strain were found to be globally lower (by 100 MPa and 0.05, respectively), despite similar microstructures and volume fractions of retained austenite.

This article further investigates the influence of the TRIP effect on the mechanical properties of two cold-rolled C-Mn-Si TRIP-assisted multiphase steels which differ by their silicon content. The purpose is to contribute to a better understanding of the factors governing the transformation of retained austenite during uniaxial tensile testing at room temperature. The influences of chemical composition and heat-treatment parameters on the stability of retained austenite will be scrutinized. It will be shown that the mechanically induced transformation of retained austenite is influenced not only by the carbon concentration of retained austenite, but also by the properties of the other phases.

II. EXPERIMENTAL PROCEDURE

The chemical compositions of the two steels are given in Table I. The composition of steel "HSi" (for "high silicon") is typical of a conventional TRIP-assisted multiphase steel with a silicon content of 1.5 wt pct. Steel "LSi" (for "low silicon") is an industrial steel grade containing a much lower silicon content. This steel is, thus, more similar to conventional cold-rolled dual-phase steel grades.[36] The microstructure and mechanical properties of steel LSi have already been reported.[33] A cast ingot of steel HSi was hot-rolled to a thickness of 4 mm following a classical procedure. Steel HSi was then cold-rolled 75 pct to 1 mm in thickness. Being an industrial steel, steel LSi was hot-rolled to a thickness of 5.5 mm following classical industrial practice. Steel LSi was subsequently cold-rolled 82 pct to the same thickness of 1 mm.

Heat treatments were carried out on 40 × 240 mm samples, with the longest dimension oriented in the rolling direction. The heat-treatment scheme is schematically represented in Figure 1. The samples were first intercritically annealed in a fluidized bed furnace. They were then transferred to a lead-bath furnace for the isothermal bainitic holding. The mean cooling rate between the two isothermal holding stages was approximately 70 °C/s. Table II summarizes the three heat-treatment conditions used for each steel grade together with the nomenclature that will be used in the remainder of the article: intercritical annealing temperature (T_1) and time (t_1) and bainite transformation temperature (T_2) and time (t_2). These heat-treatment conditions had been identified in previous work to yield favorable combinations of strength and ductility.[33,34,35]

Tensile specimens were prepared according to the European standard EN10002-1. The initial gage length was 50 mm and the width was 12.5 mm. Tensile testing was done at a crosshead speed of 2 mm/min. Measured loads and elongations were converted to true stress–true strain curves. Strain hardening was characterized by the incremental work-hardening exponent (n_{incr}), calculated from the stress-strain curves as[33]

$$n_{\text{incr}} = \frac{d \ln \sigma}{d \ln \varepsilon}$$

Because of the small grain size of ferrite (~5 to 10 μm), the Vickers microhardness of the intercritical ferrite matrix was measured using loads of 1 and 2 g in such a way as to keep the indentation size small enough in comparison to the grain size. Prior to these tests, the samples were mechanically polished with 0.25 μm diamond paste and then electrolytically polished for 10 minutes in a solution of 5 pct $HClO_4$ and 95 pct glacial acetic acid, in order to remove any work-hardened surface layer. They were finally etched with 2 pct Nital to reveal the different phases. After indentation, the diagonals and area of the impressions were measured on scanning electron microscopy (SEM) micrographs. These measurements were calibrated by carrying out the same indentation tests with 1 and 2 g loads on standards of known hardness under 10 g.

Microstructures were studied by SEM. A complete description of the procedure used for the preparation of the specimens can be found elsewhere.[37] The initial retained austenite content of the samples, as well as the evolution of the volume fraction of austenite after different extents of plastic straining, were measured by Mössbauer spectroscopy.[33] Series of tensile specimens of each heat-treatment condition were first strained to different levels ranging up

Table I. Chemical Compositions (10^{-3} wt pct) of the Investigated Steels

(10^{-3} Wt Pct)	C	Mn	Si	P	S	Cr	Ni	Cu	Nb	Al	N
HSi	130	1420	1500	13	9	13	20	8	0	27	7.9
LSi	160	1300	380	13	12	19	27	19	13	30	6.3

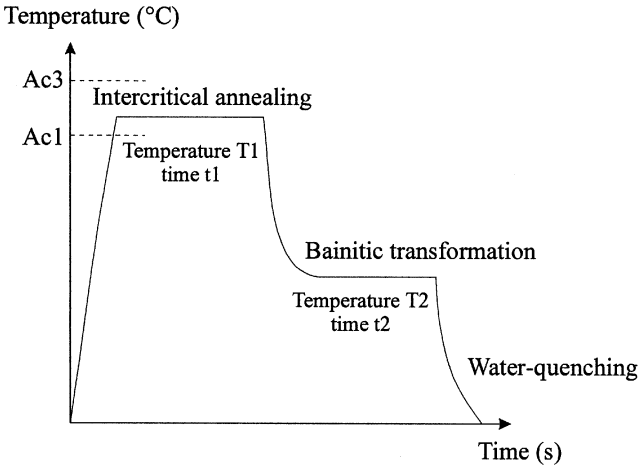

Fig. 1—Scheme of the heat treatment applied after cold rolling in order to generate a multiphase microstructure containing retained austenite.

Table II. Heat-Treatment Conditions of the Three Different Specimens of Each Steel Grade Considered in This Study

HSi	H-760-410	760 °C/2 min/410 °C/5 min
	H-775-360	775 °C/2 min/360 °C/5 min
	H-775-410	775 °C/2 min/410 °C/5 min
LSi	L-30s	730 °C/5 min/370 °C/30 s
	L-60s	730 °C/5 min/370 °C/60 s
	L-180s	730 °C/5 min/370 °C/180 s

to necking. Pieces 20-mm long were then cut from these strained specimens and chemically thinned to a thickness of 100 μm using a solution of 14 mL 40 pct HF and 100 mL 30 pct H_2O_2 diluted in 100 mL distilled water. They were then electrolytically polished at ±15 °C in a solution of 5 pct $HClO_4$ and 95 pct glacial acetic acid to a thickness of 30 to 50 μm. Reproducibility was tested by repeating the whole measurement procedure three to four times on some specific specimens.

The volume fractions of intercritical ferrite, bainite, and, possibly, thermal martensite (*i.e.*, martensite formed during quenching to room temperature after bainitic holding) were determined by combining dilatometric measurements during heat treatment and image analysis on SEM micrographs of samples quenched after intercritical annealing.[38] The grain size of retained austenite was estimated for each specimen by measuring the mean linear intercept of 300 to 500 grains on SEM micrographs. Finally, the carbon content of retained austenite was estimated from the lattice parameter measured by X-ray diffraction using Cu K_α radiation. The mean lattice parameter determined using the $(220)\gamma$ and $(311)\gamma$ peaks was converted to carbon content by using the relationship a_0 (Å) = 3.578 + 0.033 C (wt pct). The effects of manganese and silicon on the austenite lattice parameter were taken into account by using the corrections proposed by Dyson *et al.*[39]

III. RESULTS

A. *Microstructure and Mechanical Properties*

Figure 2 shows typical SEM micrographs of steel HSi after the three heat-treatment conditions considered for this steel grade. Intercritical ferrite constitutes the major phase of the microstructure, while the other phases (*i.e.*, bainite and retained austenite) are dispersed at the grain boundaries of the ferrite grains. No martensite can be found in the microstructure of specimens H-760-410 and H-775-410. However, some grains of martensite can be found in specimen H-775-360, thus indicating that M_s is near room temperature for this specimen. As indicated in Figure 2(a), two types of retained austenite can be distinguished: (1) the part of the initial intercritical austenite grains remaining intact after the partial bainite transformation ("blocky-type" austenite); or (2) films of austenite inserted between the bainite laths ("film-type" austenite). It is also noteworthy that the austenite grain size is quite small, as a consequence of the small grain size of intercritical austenite dispersed at the ferrite grain boundaries and of the partial bainite transformation that consumes part of the initial grains or divides them into several parts.

Figure 3 presents SEM micrographs of the microstructure obtained at the end of the three heat treatments considered in the case of steel LSi. For these three specimens, the intercritical temperature (730 °C) and time (5 minutes), as well as the bainitic holding temperature (370 °C), were kept identical. The nature of the second phases changed only as a consequence of the change of the bainitic holding time (30, 60, and 180 seconds, respectively). Specimens L-30s and L-60s contain martensite, while only bainite and retained austenite can be found in specimen L-180s. In addition to austenite grains at ferrite grain boundaries, steel LSi specimens also contain very small intraferritic austenite grains ("isolated-type" austenite) resulting from the intercritical annealing of cold-rolled pearlite colonies.[33]

The volume fractions of the phases constituting the microstructure of the six specimens, as well as the grain size and carbon content of retained austenite, are given in Table III. All specimens contain almost the same volume fraction of retained austenite, except specimen L-180s, which contains slightly less austenite. Intercritical ferrite is always the major phase, while the volume fractions of bainite are around 30 pct for specimens H-775-360 and H-775-410 and around 10 to 20 pct for the other specimens. Specimens L-30s and L-60s contain 5 to 10 pct of thermal martensite (resulting from the lower carbon content of retained austenite in these two specimens). Specimen L-180s corresponds to the shortest bainitic holding time at 370 °C needed to lower the M_s

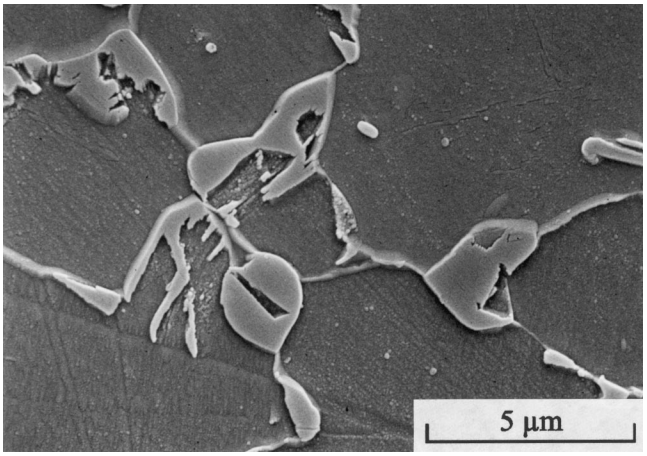

(*a*)

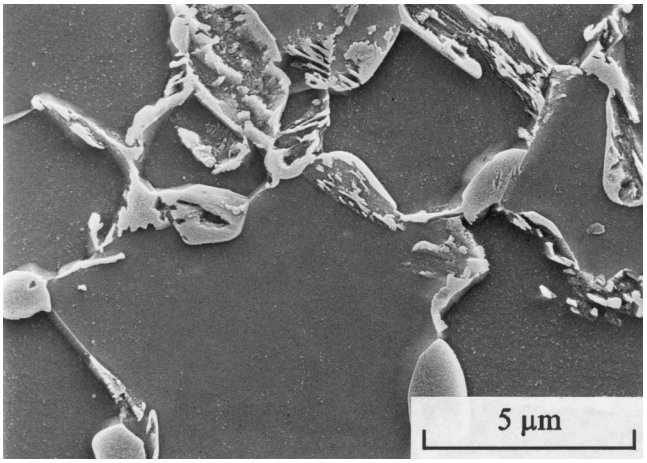

(*b*)

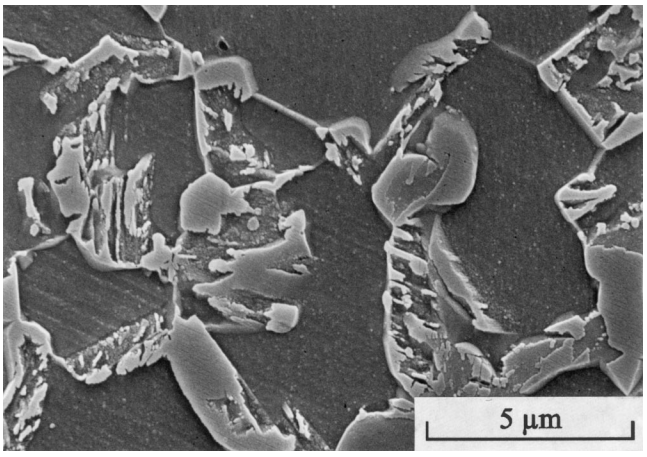

(*c*)

Fig. 2—SEM micrographs of the typical microstructure of steel HSi after the three different heat treatments: (*a*) specimen H-760-410, (*b*) specimen H-775-360, and (*c*) specimen H-775-410 (F: ferrite, A: austenite, and B: bainite).

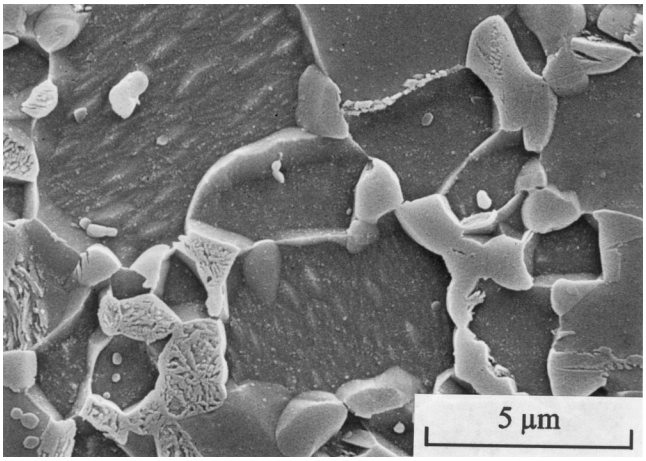

(*a*)

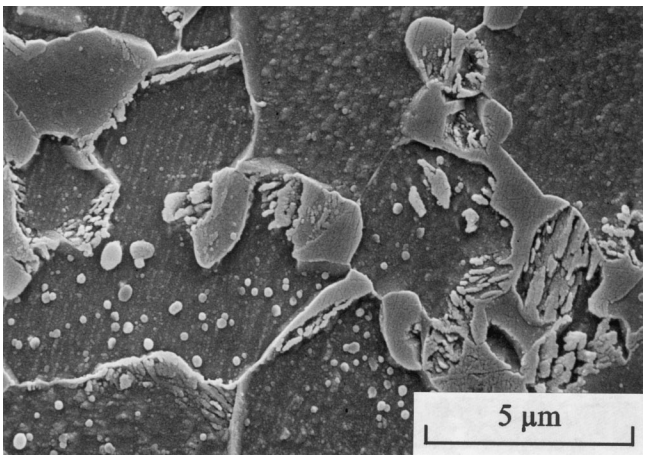

(*b*)

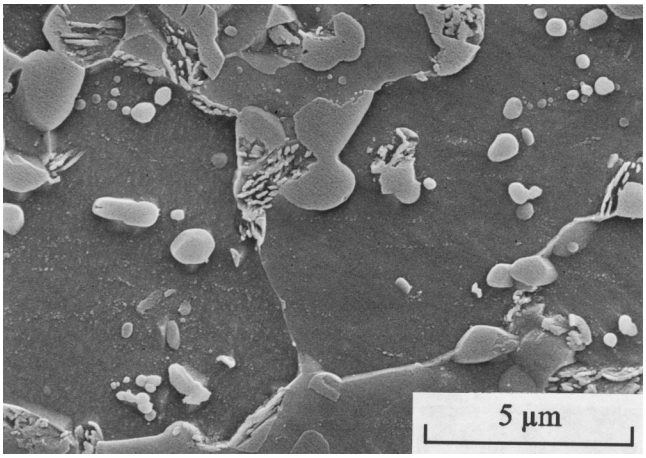

(*c*)

Fig. 3—SEM micrographs of the typical microstructure of steel LSi after the three different heat treatments: (*a*) specimen L-30s, (*b*) specimen L-60s, and (*c*) specimen L-180s (F: ferrite, A: austenite, B: bainite, and M: martensite).

temperature of steel LSi below room temperature. No martensite can be found in specimens of steel HSi, except some grains in specimen H-775-360.

Table III also gives the austenite grain size (mean linear intercept) and carbon content (estimated from the lattice parameter). While the grain size is almost the same for the different specimens (around 1.7 μm), the carbon enrichment is quite different. Specimens of steel HSi present a higher carbon enrichment of austenite than specimens of steel LSi. For specimens H-760-410 and H-775-410, the carbon content of austenite reaches the maximum level allowed for this

Table III. Volume Fractions of the Different Phases Constituting the Microstructure of Each Specimen, Carbon Content (as Estimated by X-Ray Diffraction), and Grain Size (Mean Linear Intercept) of Retained Austenite

		Ferrite (Pct)	Bainite (Pct)	Retained Austenite (Pct)	'Thermal' Martensite (Pct)	Carbon Content of Austenite (Wt Pct)	Grain Size of Austenite (μm)
HSi		±3	±3	±0.4	±1	±0.03	—
	H-760-410	75	17	8	0	0.93	2.0 ± 0.7
	H-775-360	60	32	7.9	~0	0.85	1.6 ± 0.6
	H-775-410	60	32	7.8	0	0.97	1.6 ± 0.6
LSi							
	L30s	75	9	8.8	7	0.61	1.7 ± 0.6
	L-60s	75	12	8.1	5	0.68	1.8 ± 0.7
	L-180s	75	19	6.1	0	0.73	1.5 ± 0.6

steel composition by the T_0 curve at 410 °C.[38] For steel LSi, the carbon enrichment is lower because of the loss of carbon by partial carbide precipitation.[38] The carbon content of austenite in specimen L-30s is only somewhat higher than the level estimated by considering that all carbon concentrates in the 25 pct intercritical austenite formed at 730 °C. A longer bainitic holding time is accompanied by a carbon enrichment of austenite. After 3 minutes, the austenite in steel LSi becomes sufficiently carbon-rich that it does not transform to martensite during cooling to room temperature. In summary, the different specimens present the same volume fraction of austenite with identical grain size, but different carbon enrichments and different phases surrounding the austenite grains.

Figures 4(a) and (b) present the true stress–true strain curves of the six specimens. Steel HSi (Figure 4(a)) exhibits better mechanical properties than steel LSi, *i.e.*, higher true stresses at maximum loads and larger true uniform strains. Specimen H-775-360 presents the highest true stress at maximum load but a lower true uniform strain than specimens H-760-410 and H-775-410. The best strength-ductility combination is obtained with specimen H-760-410. For steel LSi (Figure 4(b)), it can be seen that, when the bainitic holding time increases from 30 to 180 seconds, the true stress at maximum load decreases and the yield strength increases. Specimen L-60s, with the intermediate bainite transformation time, presents the largest true uniform strain for steel LSi.

Figure 5 presents the variation of the incremental work-hardening exponent n_{incr} as a function of strain. The straight line corresponds to the instability criterion $\varepsilon_u = n_{\text{incr}}$, where ε_u is the true strain at the onset of necking. It appears that the different strength-ductility combinations are associated with completely different work-hardening behaviors. The large true uniform strains of specimens H-760-410 and H-775-410 are associated with a high, slightly increasing incremental work-hardening exponent during the entire straining. Specimen H-775-360 presents a higher value of n_{incr} after the Lüders plateau than specimens H-760-410 and H-775-410. However, this high initial level in specimen H-775-360 does not persist, and the progressive decrease of n_{incr} induces an earlier onset of necking. In comparison to steel HSi, specimens of steel LSi present a completely different evolution of hardening during plastic straining. For specimens L-30s and L-60s, n_{incr} first increases to very high values (0.3 to 0.35) after the onset of yielding and, thereafter, steeply decrease to values lower than for the specimens of steel HSi. In summary, the best mechanical properties with a delayed onset of necking correspond to an initially low value

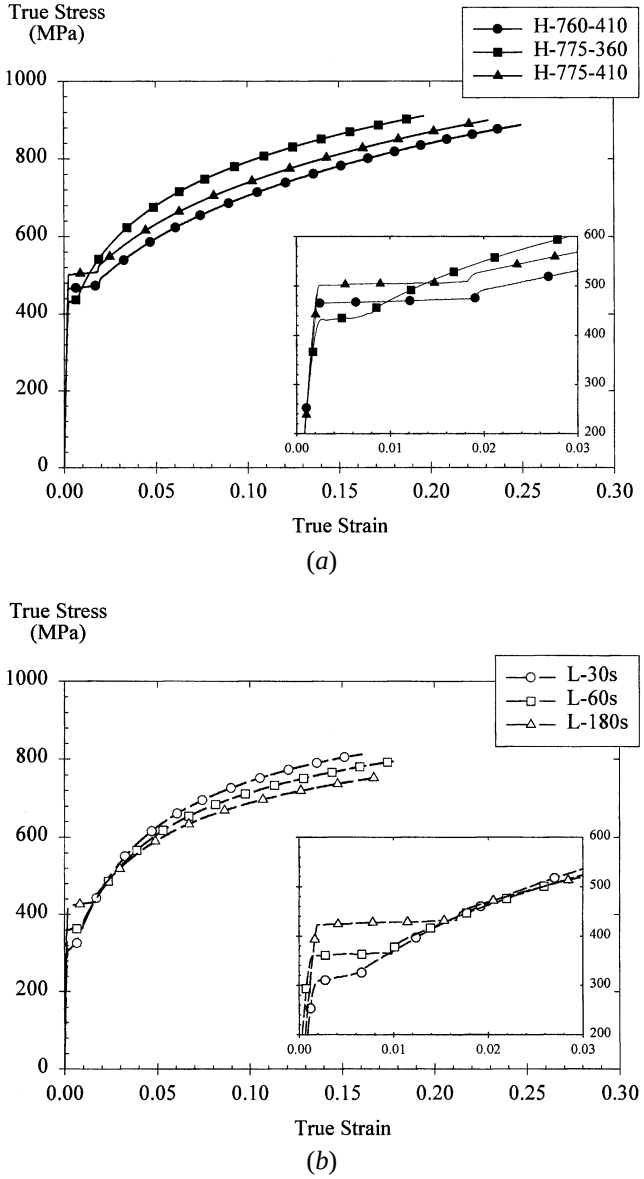

Fig. 4—True stress–true strain curves of (*a*) the specimens of steel HSi and (*b*) the specimens of steel LSi.

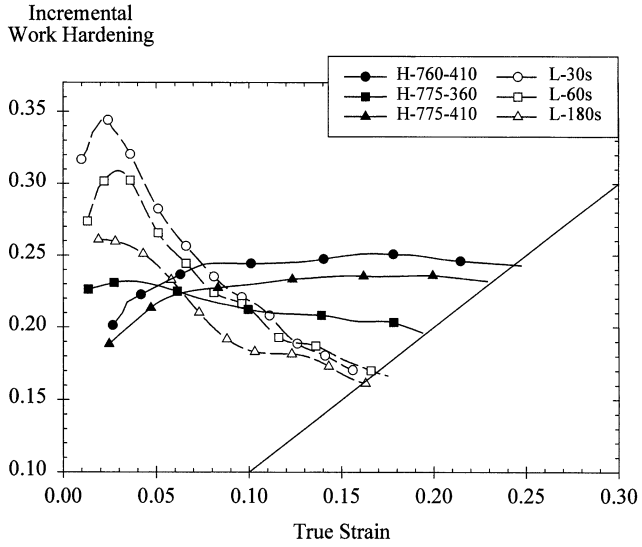

Fig. 5—Incremental work-hardening curves (n_{incr}) of the different specimens of steels HSi and LSi.

of n_{incr}, which increases in steel HSi, and to the highest initial value of n_{incr} for steel LSi.

The microhardness of the intercritical ferrite grains of the two steel grades has been measured. For steel HSi, specimen H-760-410 was chosen. For steel LSi, measurements were made on specimen L-180s in order to avoid any possible effect of the presence of internal stresses generated by the formation of martensite during cooling (thermal martensite). Up to 100 measurements were made in each case. The measured hardness is 187.1 ± 6.2 kg/mm^2 in steel HSi, whereas it is 168.4 ± 5.1 kg/mm^2 in steel LSi. The hardness of the ferrite matrix is, thus, significantly higher in steel HSi than in steel LSi.

B. *Variation of Retained Austenite Volume Fraction as a Function of Plastic Strain*

Figures 6(a) and (b) present the evolution of the retained austenite content with plastic strain for each heat-treatment condition of steels HSi and LSi. Even though all specimens contain about the same initial content of retained austenite, the rate of austenite transformation during plastic straining is different. The retained austenite content decreases more slowly for specimens of steel HSi (Figure 6(a)). For specimens H-760-410 and H-775-410, austenite transforms very progressively with plastic strain, while the decrease is somewhat faster for specimen H-775-360 and for the three specimens of steel LSi (Figure 6(b)). The fastest austenite transformation rate is observed for specimens L-30s and L-180s. It is noteworthy that a large part of austenite remains untransformed when the specimens have been strained up to the onset of necking. This is more clearly seen in Figure 7, which presents the variation of the proportion of retained austenite transformed to martensite ($1 - V\gamma_r/V\gamma_{r0}$) as a function of normalized strain ($\varepsilon/\varepsilon_u$). For specimens of steel HSi, only 50 to 60 pct of the initial volume fractions of austenite transform before the onset of necking, while this proportion is larger for steel LSi (between 65 and 80 pct). Figure 7 better illustrates that austenite transforms very progressively for specimens H-760-410 and H-775-410, but

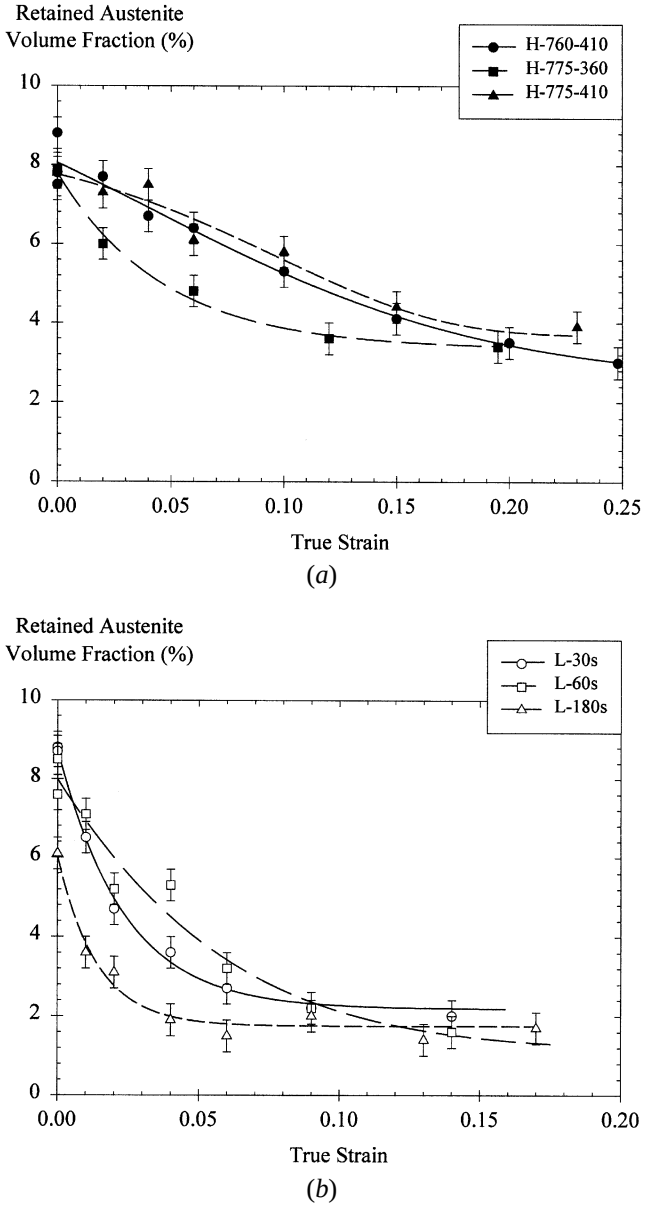

Fig. 6—Retained austenite content as a function of true strain for specimens of (*a*) steel HSi and (*b*) steel LSi.

very much faster for specimens L-30s and L-180s. For these two latter specimens, all the "transformable" retained austenite is already transformed after only 30 pct of the true uniform strain.

In order to estimate the transformation rate of retained austenite during plastic straining, Figure 8 presents an exponential fit of the variations of the normalized transformable austenite, according to

$$\frac{V\gamma - V\gamma_{\varepsilon_u}}{V\gamma_0 - V\gamma_{\varepsilon_u}} = ke^{-n\varepsilon}$$

where $V\gamma_{\varepsilon u}$ is the volume fraction of retained austenite remaining untransformed at true uniform strain, $V\gamma_0$ is the initial volume fraction of retained austenite, and k and n are constants. The transformation rate can, thus, be shortly expressed by the n parameter.

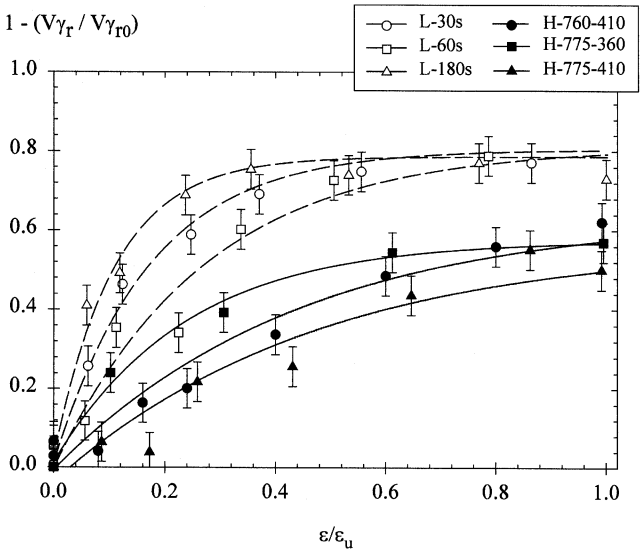

Fig. 7—Proportion of transformed austenite as a function of true strain normalized by true uniform strain of the specimens of steels HSi and LSi, respectively.

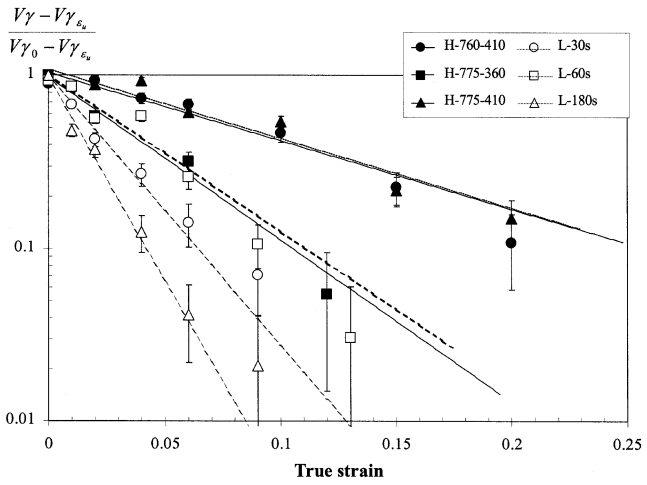

Fig. 8—Variations of the transformable austenite as a function of true strain for the different specimens of steels HSi and LSi. The straight lines correspond to the exponential fits.

Figure 8 shows that specimens H-760-410 and H-775-410 exhibit a low transformation rate, whereas specimens H-775-360 and L-60s exhibit similar transformation rates, slightly higher than for specimens H-760-410 and H-775-410. The transformation rates are very high for specimens L-30s and L-180s. It is striking that specimen L-180s, which contains a higher austenite carbon content than specimens L-30s and L-60s (Table III), transforms very rapidly, like specimen L-30s.

Figure 9 presents micrographs of specimens of steel HSi strained up to the onset of necking. It suggests that the untransformed part of austenite corresponds to the interlath austenite film associated with bainitic ferrite (the film-type austenite). As shown in Figure 10, the isolated type of retained austenite (dispersed inside intercritical ferrite grains) present in steel LSi also remains untransformed at the onset of necking.

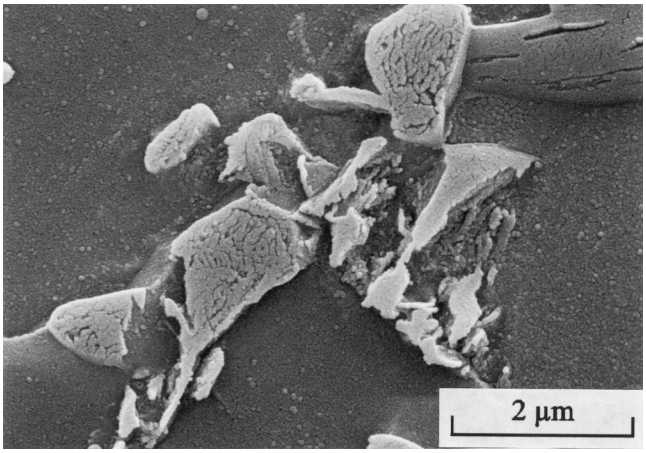

(*a*)

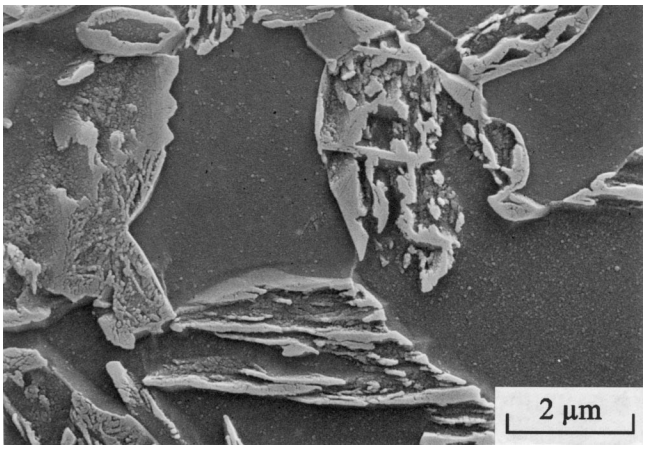

(*b*)

Fig. 9—(*a*) and (*b*) SEM micrographs showing the not transformed retained austenite associated with bainite in the case of specimens H-760-410 and H-775-360 after tensile testing up to true uniform strain.

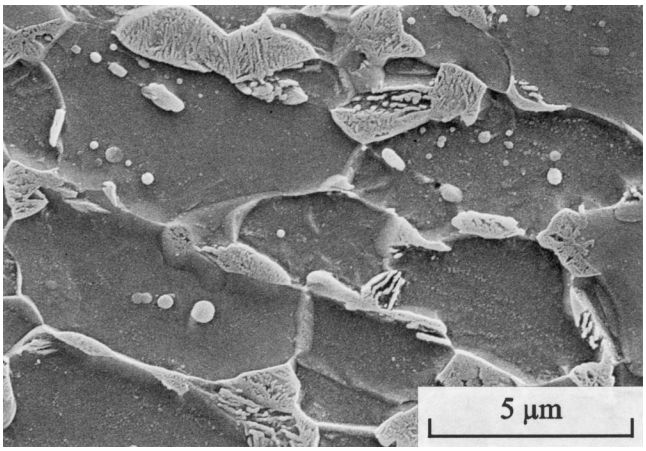

Fig. 10—SEM micrograph of specimen L-60s after tensile testing up to true uniform strain.

IV. DISCUSSION

The heat treatments presented here have been chosen in such a way as to generate microstructures containing almost the same amount of retained austenite in spite of the different

silicon contents of steels HSi and LSi. Furthermore, measurements have shown that the average grain sizes of retained austenite are not significantly different in these specimens. However, these specimens differ by the carbon content of retained austenite and by the nature and volume fractions of the phases constituting the "matrix" in which the austenite grains are dispersed (Table III). These two differences seem to influence in a large way the true stress–true strain curves (Figures 4) and, particularly, the evolution of the incremental work-hardening exponent n_{incr} (Figure 5).

It is widely admitted that the resistance of austenite to martensitic transformation and, particularly, the mechanical stability of retained austenite depend on its grain size[40,41] and carbon content.[27,30,42] In the present case, the average austenite grain size can be considered to be identical in all specimens, so that this parameter cannot explain the differences observed for the austenite mechanical stability. As carbon is the best austenite stabilizer, a more carbon-rich austenite has a lower M_s temperature, and the work for triggering the martensitic transformation has, thus, to be increased. The mechanically induced martensitic transformation, therefore, occurs later during straining. Figure 11 presents, for the six specimens of steels HSi and LSi, the transformation rate of transformable austenite (expressed by the parameter *n*, determined by the exponential fitting of Figure 8) as a function of the carbon content of retained austenite. For the three specimens of steel HSi (bold symbols), the continuous line in this figure points toward the apparent correlation between the carbon content of retained austenite and its resistance to martensitic transformation. Nevertheless, the specimens of steel LSi (open symbols) do not follow this correlation line. The stability of austenite in these steels, thus, appears to depend also on other characteristics of the microstructure.

A comprehensive interpretation of the mechanisms by which the interactions between the various phases constituting the microstructure affect austenite stability would necessitate a micromechanical model based, for example, on Eshelby's inclusion theory[43,44] extended to elastoplastic behavior[45,46,47] or using computational cell models. The development of such a model is out of the scope of this article. However, a qualitative insight may be gained by resorting to basic principles and existing results of the mechanics of composite elastoplastic materials. In TRIP-assisted multiphase steels, the flow strength of retained austenite is higher than the flow strength of both intercritical ferrite and bainite.[48] The present microstructures can be considered to consist of a discontinuous composite in which the austenite grains constitute the reinforcing phase dispersed in a ferrite-based matrix (composed of a mixture of intercritical ferrite, bainite, and martensite) that globally presents a lower flow strength than the reinforcement particles. As shown by Bao *et al.*,[49] isostrain conditions (Voigt assumption) prevail during plastic straining of discontinuous composites, as long as the flow stress of the reinforcement particles is not larger than twice the flow stress of the matrix. There is little doubt that most of the TRIP effect occurs while both the austenite grains and the multiphase matrix in which these grains are dispersed are flowing plastically, which means that the strain-induced transformation regime dominates during most of the tensile test. As the flow stress of austenite grains is not larger than twice the flow stress

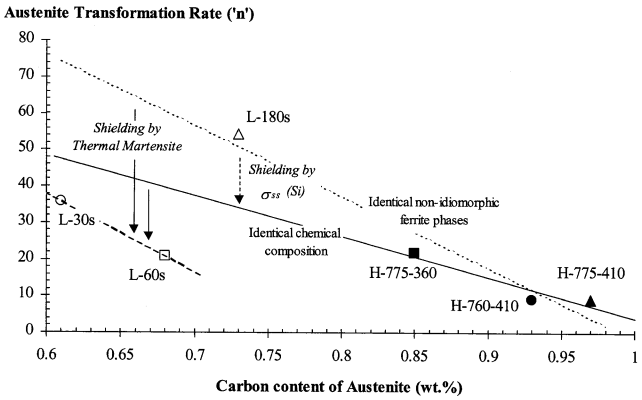

Fig. 11—Transformation rate of austenite (expressed by the parameter *n* of the exponential fitting of Fig. 8) as a function of the carbon content of retained austenite in the specimens of steels HSi and LSi (continuous line: linear fitting of the three specimens of steel HSi (identical chemical composition); and dotted line: linear fitting of the three specimens of steel HSi and specimen L-180s (identical nature of the nonintercritical ferrite phases)).

of the matrix,[48] the stress partition between the austenite grains and the surrounding matrix during plastic straining can be estimated by assuming isostrain conditions.

For the three specimens of steel LSi, which differ only by the bainite transformation time, the increase of the carbon content of retained austenite with increasing transformation time brings about a progressive decrease of the content of thermal martensite (Table III). As a guide for the eye, the dotted line in Figure 11 is a correlation line drawn for the four specimens L-180s, H-775-360, H-760-410, and H-775-410, which contain similar microstructures consisting of ferrite, bainite, and retained austenite (with different levels of carbon), but no thermal martensite. The transformation rate (*n*) of specimens L-30s and L-60s is much lower than the rate extrapolated according to this correlation line. It is, thus, tempting to ascribe this lower transformation rate to the presence of thermal martensite in the matrix. The presence of hard martensite grains in the matrix can be assimilated to a strengthening of this matrix that leads to a change in the partition of the stress between the constitutive phases. Following the work of Bao *et al.*,[49] a stronger matrix, thus, leads to a smaller mean-stress level within the austenite grains and, thus, to a postponed triggering of the martensitic transformation. Furthermore, since the equivalent stress (directly related to the equivalent strain) is not changed while the mean stress decreases, the stress triaxiality within the austenite grains also decreases. As shown by Jacques *et al.*,[50] a decrease of stress triaxiality causes a decrease of the austenite transformation rate. The strengthening of the matrix by martensite, thus, brings about a sort of "shielding" effect that causes a decrease of the austenite transformation rate: despite a much lower carbon content, the retained austenite in specimen L-60s exhibits an apparent mechanical stability that is comparable to that of specimen H-775-360. It is worth noticing that this behavior is different from the behavior reported for fully austenitic TRIP steels, in which, as modeled by Stringfellow *et al.*,[10] a higher strength of austenite (which, in that case, was considered to be the matrix) increases the martensitic transformation rate.

A similar composite model could be used for interpreting the influence of the silicon content of intercritical ferrite on

the apparent mechanical stability of retained austenite. Since the intercritical annealing time is too short to induce redistribution of substitutional elements (paraequilibrium conditions[51]), the ferrite matrix in steels HSi and LSi contains 1.5 and 0.38 wt pct of silicon, respectively. Silicon is known as being a potent solid-solution strengthening addition for ferrite.[52,53] This justifies the microhardness measurements: intercritical ferrite is harder in specimen H-760-410 than in specimen L-180s. Actually, the composition of steel LSi is typical of cold-rolled dual-phase steels, and the hardness of the ferrite matrix measured in the present study is in good agreement with published results on dual-phase steels.[54,55] The ferrite yield strength may be estimated from these hardness values by considering that, for a rigid-plastic material indented by a Vickers indenter, the yield strength is approximately one-third of the hardness ($\sigma_y \sim H_v/3$).[56,57] This means that, due to the higher concentration of silicon, the ferrite yield strength would be higher by about 65 MPa in steel HSi than in steel LSi. This difference is in good agreement with the solid-solution strengthening effect of silicon predicted by Leslie,[58] Sugden *et al*,[59] and Pickering *et al*,[52,53,60] who proposed a strengthening effect by silicon of the order of 100 MPa for 1 wt pct of solute. On the other hand, it seems that the solid-solution strengthening effect of silicon is much smaller in austenite: Pickering[53] and Aranzabal[61] report a strengthening effect by silicon in austenite of the order of 20 MPa for 1 wt pct of solute. It can, therefore, be anticipated that the stress partition between austenite grains and the surrounding matrix depends on the silicon content of the specimens: the solid-solution strengthening effect of silicon would indirectly contribute to the apparent mechanical stability of retained austenite in the HSi steels. This interpretation could justify the fact that, as hinted in Figure 11, the transformation rate in specimen L-180s appears to be higher than the rate extrapolated on the basis of the (continuous) correlation line corresponding to the transformation rates measured for the three specimens with a high silicon content.

Although intercritical ferrite is always the major phase in TRIP-assisted multiphase steels, hardly any consideration has been given in the literature to the influence of the mechanical properties of ferrite.[23] Many studies have aimed at tuning the volume fraction and stability of retained austenite in TRIP-aided steels by changing the amount of silicon (from 1 to 2.5 wt pct).[23,27,28,42] None of these studies have considered the solid-solution strengthening effect of silicon. We propose that the austenite stabilizer effect ascribed to silicon,[27,42] which leads to the exceptional combination of strength and ductility of the conventional TRIP-assisted multiphase steels, could also partly result from the higher strength of the more silicon-rich intercritical ferrite matrix.

It has been shown in Figure 7 that, in the three specimens of steel HSi, 40 to 50 pct of the initial amount of retained austenite remains untransformed at the onset of necking. Figure 9 confirms that, as already observed by Sugimoto *et al.*[31] and Itami *et al*,[32] the film-type austenite located between bainitic ferrite laths cannot easily transform during straining. Indeed, the carbon enrichment of austenite is the highest along the broad face of the bainitic ferrite platelets.[62,63] Furthermore, this film-type austenite presents a smaller grain size, which could play a stabilizing effect. This stabilization due to small grain size could also explain the absence of transformation of intragranular retained austenite in steel LSi. The parts of retained austenite untransformed at the onset of necking in steels HSi and LSi are, thus, related to the proportion of bainite and to the proportion of intragranularly dispersed austenite, respectively.

V. CONCLUSIONS

This study aimed at scrutinizing the factors contributing to the mechanical stability of retained austenite in two TRIP-assisted multiphase steels which differed by their silicon content. Different specimens were considered, for which the initial content and the grain size of retained austenite were similar. It was shown that mechanical properties are drastically affected by interactions between the phases. When austenite is a dispersed phase in a ferrite-based multiphase microstructure, its strain-induced transformation rate also depends on the stress partitioning between austenite and the surrounding phases. The resulting "apparent" stability of retained austenite will, thus, depend not only on austenite properties but also on the properties of the other phases.

In the case of the low-silicon steel LSi, the thermal martensite formed during cooling to room temperature increases ferrite strain hardening in such a way as to bring about a *shielding effect*, reducing the rate of stress increase in austenite. This effect somewhat compensates for the limited stability of austenite due to the low carbon enrichment. It is proposed that the solid-solution strengthening effect due to silicon leads to a higher stress partition toward the intercritical ferrite matrix and, thus, also to another type of shielding of retained austenite. The mechanical stability of retained austenite, thus, appears to be influenced by the mechanical properties of the surrounding matrix in a more complex way than previously considered in the literature.

ACKNOWLEDGMENTS

The authors are indebted to R&D Cockerill-Sambre (Usinor Group) for continuous support. The work of PJJ was supported by the Fonds National de la Recherche Scientifique (Belgium) and by a fellowship of the Government of Québec for a postdoctoral period at McGill University. This work was partly supported by the Belgian State, Prime Minister's Office, Federal Office for Scientific, Technical and Cultural Affairs, under Contract No. P4/33 Inter-University Poles of Attraction Programme.

REFERENCES

1. J.R. Patel and M. Cohen: *Acta Metall.*, 1953, vol. 1, pp. 531-38.
2. T. Angel: *J. Iron Steel Inst.*, 1954, pp. 165-74.
3. V.F. Zackay, E.R. Parker, D. Fahr, and R. Busch: *Trans. Am. Soc. Met.*, 1967, vol. 60, pp. 252-59.
4. D.C. Ludwigson and J.A. Berger: *J. Iron Steel Inst.*, 1969, pp. 63-69.
5. G.B. Olson and M. Cohen: *Metall. Trans. A*, 1975, vol. 6A, pp. 791-95.
6. H. Onodera, H. Goto, and I. Tamura: *Proc. 1st JIM Int. Symp. New Aspects of Martensitic Transformations*, Kobe, Japan, 1976, pp. 327-38.
7. G.B. Olson and M. Azrin: *Metall. Trans. A*, 1978, vol. 9A, pp. 713-21.
8. G.B. Olson and M. Cohen: *Metall. Trans. A*, 1982, vol. 13A, pp. 1907-14.
9. G.B. Olson: in *Deformation, Processing and Structures*, G. Krauss, ed. ASM, Metals Park, OH, 1982, pp. 391-424.
10. R.G. Stringfellow, D.M. Parks, and G.B. Olson: *Acta Metall. Mater.*, 1992, vol. 40 (7), pp. 1703-16.

11. I. Tamura and C.M. Wayman: in *Martensite*, G.B. Olson and W.S. Owen, eds., ASM, Metals Park, OH, 1992, pp. 227-42.
12. J.B. Leblond, J. Devaux, and J.C. Devaux: *Int. J. Plasticity*, 1989, vol. 5, pp. 551-72.
13. F. Marketz and F.D. Fischer: *Metall. Trans. A*, 1995, vol. 26A, pp. 267-78.
14. C.L. Magee and H.W. Paxton: *Trans. TMS-AIME*, 1968, vol. 242, pp. 1741-49.
15. G.W. Greenwood and R.H. Johnson: *Proc. R. Soc. London, Ser. A*, 1965, vol. 283, pp. 403-22.
16. D. Fahr: *Metall. Trans.*, 1971, vol. 2, pp. 1883-92.
17. D. Bhandarkar, V.F. Zackay, and E.R. Parker: *Metall. Trans.*, 1972, vol. 3, pp. 2619-31.
18. R.B.G. Yeo: *Trans. TMS-AIME*, 1963, vol. 227, pp. 884-90.
19. G.R. Chanani, V.F. Zackay, and E.R. Parker: *Metall. Trans.*, 1971, vol. 2, pp. 133-39.
20. Y. Sakuma, O. Matsumura, and O. Akisue: *Iron Steel Inst. Jpn. Int.*, 1991, vol. 31, pp. 1348-53.
21. O. Matsumura, Y. Sakuma, and H. Takechi: *Scripta Metall.*, 1987, vol. 21, pp. 1301-06.
22. Y. Sakuma, D.K. Matlock, and G. Krauss: *Metall. Trans. A*, 1992, vol. 23A, pp. 1221-32.
23. K. Sugimoto, N. Usui, M. Kobayashi, and S. Hashimoto: *Iron Steel Inst. Jpn. Int.*, 1992, vol. 32, pp. 1311-18.
24. W.C. Jeong, D.K. Matlock, and G. Krauss: *Mater. Sci. Eng. A*, 1993, vol. 165, pp. 1-8.
25. H.K.D.H. Bhadeshia: *Bainite in Steels*, The Institute of Materials, London, 1992, pp. 61-87.
26. H.K.D.H. Bhadeshia and D.V. Edmonds: *Metall. Trans. A*, 1979, vol. 10A, pp. 895-907.
27. I. Tsukatani, S. Hashimoto, and T. Inoue: *Iron Steel Inst. Jpn. Int.*, 1991, vol. 31, pp. 992-1000.
28. O. Matsumura, Y. Sakuma, Y. Ishii, and J. Zhao: *Iron Steel Inst. Jpn. Int.*, 1992, vol. 32, pp. 1110-16.
29. Y. Sakuma, D.K. Matlock, and G. Krauss: *Metall. Trans. A*, 1992, vol. 23A, pp. 1233-41.
30. A. Itami, M. Takahashi, and K. Ushioda: *Iron Steel Inst. Jpn. Int.*, 1995, vol. 35, pp. 1121-27.
31. K. Sugimoto, M. Misu, M. Kobayashi, and H. Shirasawa: *Iron Steel Inst. Jpn. Int.*, 1993, vol. 33, pp. 775-82.
32. A. Itami, M. Takahashi, and K. Ushioda: *Proc. Symp. High-Strength Steels for Automotive Industry*, C.E. Slater, Baltimore, MD, 1994, pp. 245-54.
33. P. Jacques, X. Cornet, P. Harlet, J. Ladrière, and F. Delannay: *Metall. Mater. Trans. A*, 1998, vol. 29A, pp. 2383-93.
34. P. Jacques, K. Eberle, P. Harlet, and F. Delannay: *Proc. 40th Mechanical Working & Steel Processing Conf.*, Pittsburgh, PA, Oct. 25–28, 1998, ISS, Warrendale, PA, pp. 239-50.
35. P. Jacques, E. Girault, P. Harlet, and F. Delannay: *Iron Steel Inst. Jpn. Int.*, 2001, vol. 41, pp. 1061-67.
36. G.R. Speich: in *Fundamentals of Dual Phase Steels*, R.A. Kot and B.L. Bramfitt, eds., TMS-AIME, Warrendale, PA, 1981, pp. 3-45.
37. E. Girault, P. Jacques, K. Mols, P. Harlet, J. van Humbeeck, E. Aernoudt, and F. Delannay: *Mater. Characterization*, 1998, vol. 40 (2), pp. 111-18.
38. P. Jacques, E. Girault, T. Catlin, T. Kop, N. Geerlofs, S. Van der Zwaag, and F. Delannay: *Mater. Sci. Eng. A*, 1999, vols. 273–275, pp. 475-79.
39. D.J. Dyson and B. Holmes: *J. Iron Steel Inst.*, 1970, vol. 208, pp. 469-74.
40. C.L. Magee: *Metall. Trans.*, 1971, vol. 2, pp. 2419-25.
41. G.N. Haidemenopoulos, G.B. Olson, and M. Cohen: *Proc. 34th Sagamore Army Materials Research Conf.*, Lake George, New York, NY, U.S. Government Printing Office, 1987, pp. 549-93.
42. Y. Sakuma, O. Matsumura, and H. Takechi: *Metall. Trans. A*, 1991, vol. 22A, pp. 489-98.
43. Rudiono and Y. Tomota: *Acta Mater.*, 1997, vol. 45 (5), pp. 1923-29.
44. G.J. Weng: *J. Mech. Phys. Solids*, 1990, vol. 38, pp. 419-41.
45. N.C. Goel, S. Sangal, and K. Tangri: *Metall. Trans. A*, 1985, vol. 16A, pp. 2013-23.
46. B. Karlsson and B. Sundström: *Mater. Sci. Eng. A*, 1974, vol. 16, pp. 161-66.
47. M.H. Poech and H.F. Fischmeister: *Acta Metall.*, 1992, vol. 40 (3), pp. 487-94.
48. Q. Furnemont, M. Kempf, P. Jacques, and M. Goken: *Mater. Sci. Eng. A*, in press.
49. G. Bao, J.W. Hutchinson, and R.M. McMeeking: *Mech. Mater.*, 1991, vol. 12, pp. 85-94.
50. P. Jacques, Q. Furnemont, T. Pardoen, and F. Delannay: *Acta Mater.*, 2001, vol. 49 (1), pp. 139-52.
51. M. Hillert: in *Phase Equilibria, Phase Diagrams and Phase Transformations*, M. Hillert, ed., Cambridge University Press, Cambridge, United Kingdom, 1998, pp. 348-67.
52. F.B. Pickering: *Materials Science and Technology–Vol. 7: Constitution and Properties of Steels*, F.B. Pickering, ed., VCH Publ., Weinheim, 1992, pp. 41-94.
53. F.B. Pickering: *Physical Metallurgy and the Design of Steels*, Applied Science Publishers, London, 1978.
54. A.R. Marder: in *Formable HSLA and Dual-Phase Steels*, A.T. Davenport, ed., TMS-AIME, Warrendale, PA, 1977, pp. 87-98.
55. Q.A. Chen, R. Kaspar, and O. Pawelski: *Z. Metallkd.*, 1985, vol. 76, pp. 348-52.
56. B.W. Mott: *Micro-Indentation Hardness Testing*, Butterworth and Co., London, 1956, pp. 1-15.
57. G.F. Vander Voort: *Metallography: Principles and Practice*, McGraw-Hill, New York, NY, 1984, pp. 334-83.
58. W.C. Leslie: *Metall. Trans.*, 1972, vol. 3, pp. 5-26.
59. A.A.B. Sugden and H.K.D.H. Bhadeshia: *Metall. Trans. A*, 1988, vol. 19A, pp. 1597-1602.
60. F.B. Pickering: in *Hardenability Concepts with Applications to Steel*, DV. Doane and J.S. Kirkaldy, eds., TMS-AIME, Warrendale, PA, 1977, pp. 179-225.
61. J. Aranzabal, I. Gutierrez, J.M. Rodriguez-Ibabe, and J.J. Urcola: *Metall. Trans. A*, 1997, vol. 28A, pp. 1143-56.
62. L.C. Chang and H.K.D.H. Bhadeshia: *Mater. Sci. Technol.*, 1995, vol. 11, pp. 874-81.
63. H.K.D.H. Bhadeshia and D.V. Edmonds: *Acta Metall.*, 1980, vol. 28, pp. 1265-73.